Korea-Australia Rheology Journal
Vol. 12, No. 2, June 2000 pp. 107-117

Three-dimensional numerical simulation for the prediction of product shape in sheet casting process

Kyung Sun Chae[1], Mi Hye Lee[2], Seong Jae Lee[3] and Seung Jong Lee*
School of Chemical Engineering, Seoul National University, Seoul 151-742, Korea
[1]Agency for Technology and Standards, Kwacheon 427-010, Korea
[2]Korea Technology Credit Guarantee Fund, Pusan 600-014, Korea
[3]Department of Polymer Engineering, The University of Suwon, Suwon 445-743, Korea
(Received July 4, 2000; final revision received September 16, 2000)

Abstract

Prediction of the product shape in sheet casting process is performed from the numerical simulation. A three-dimensional finite element method is used to investigate the flow behavior and to examine the effects of processing conditions on the sheet produced. Effects of inertia, gravity, surface tension and non-Newtonian viscosity on the thickness profile of the sheet are considered since the edge bead and the flow patterns in the chill roll region have great influence on the quality of the products. In the numerical simulation with free surface flows, the spine method is adopted to update the free surface, and the force-free boundary condition is imposed along the take-up plane to avoid severe singularity problems existing at the take-up plane. From the numerical results of steady isothermal flows of a generalized Newtonian fluid, it is shown that the draw ratio plays a major role in predicting the shape of the final sheet produced and the surface tension has considerable effect on the bead thickness ratio and the bead width fraction, while shear-thinning and/or tension-thickening viscosity affect the degree of neck-in.

Keywords : sheet casting process, finite element method, draw ratio, neck-in, bead thickness ratio, bead width fraction

1. Introduction

The polymer processings such as fiber spinning, film and sheet casting, curtain coating, and film blowing can be mostly described by elongational flows. Out of various processings, the sheet casting process has its importance in manufacturing polymeric films and sheets. The flow characteristic in sheet casting is planar, generally considered to be a three-dimensional flow, and shows mixed, both planar and uniaxial, elongational flow behavior. A simplified processing diagram of sheet casting process is shown in Fig. 1. A molten polymer is extruded through a flat slit die to form a sheet and then stretched in air at a distance between the die-exit and the chill roll which quenches the melt and solidifies it for wind-up. The longitudinally stretched sheet passes over cooled stabilizing rolls before progressing to a preheating zone for drawing and orientation in the transverse direction. Indeed, the sheet develops an edge and forms an edge bead, and eventually the thick edge on the frozen sheet is trimmed off and recycled. The take-up velocity at the chill roll is greater than the extrusion velocity at the die. The ratio of the cross-sectional area of the sheet emerging from the die-exit to that of the sheet at the chill roll is defined as the draw ratio. For incompressible fluids, this is equal to the ratio of the take-up to extrusion velocities.

The film and sheet casting process has long been studied for the two-dimensional problems of Newtonian fluids (d'Halewyn et al., 1990; Song, 1993) and of viscoelastic fluids (Alaie and Papanastasiou, 1991; Debbaut and Marchal, 1995). These studies allow modeling of the well-known edge bead defect but cannot obtain the shape of complete edge bead. It was shown that the resulting viscoelastic films get thin and velocities increase abruptly just downstream of the die-exit compared to the Newtonian films. In the film casting process, the edge bead is difficult to handle, the film cannot be wound properly, and the mechanism forming the edge bead is not clear yet. The causes of edge bead were studied by Dobroth and Erwin (1986). Three causes of edge bead were discussed: surface tension, die swell and edge stress effect. They predicted that the predominant cause of edge bead is an edge stress effect and this effect is a result of the difference in a way that the edge and center are stretched. The stability analysis on draw resonance was performed for the isothermal

*Corresponding author: sjlee@plaza.snu.ac.kr
© 2000 by The Korean Society of Rheology

Newtonian extending film and sheet (Yeow, 1974) and extended to the isothermal viscoelastic film casting (Anturkar *et al.*, 1988). These studies indicate that shear-thinning fluids are less stable and fluids with higher fluid characteristic time are more stable. Recently, a Newtonian, isothermal time-dependent two-dimensional model, constituted of an elastic-like equation for velocity coupled to a transport equation for thickness and a free surface computation, was developed (Silagy *et al.*, 1999), and the onset of the draw resonance instability was studied.

The uniform thickness of the film is of prime importance in the industrial sheet casting process. In this work, we would like to consider the effects of the three-dimensional flow behavior in sheet casting in order to observe the sheet profile carefully. Singular stress may appear on the chill roll region and flows with stress singularities pose obstacles to numerical simulations. A proper mathematical representation of the boundary condition at that region is required for numerical computations. It is also important to know at the design stage the causes of edge bead to select proper operating condition, and to control the flow pattern by processing steps. It is hard, however, to predict these behavior from a process, since they are strongly affected by several conditions in processing steps. Therefore, the effects of draw ratio, inertia, gravity, surface tension and the rheological properties of the generalized Newtonian fluid are examined with three-dimensional numerical simulations.

2. Problem description

2.1. Governing equations

A planar sheet of polymer is extruded through a die of thickness $2H_o$ and width $2W_o$, and is continuously taken-up at the chill roll, by a constant velocity u_L, which is greater than the extrusion velocity u_o as shown in Fig. 2. The fluid

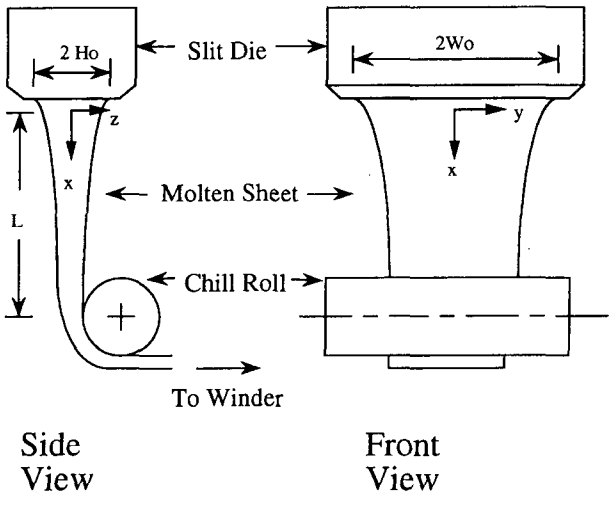

Fig. 1. Schematic diagram of sheet casting process.

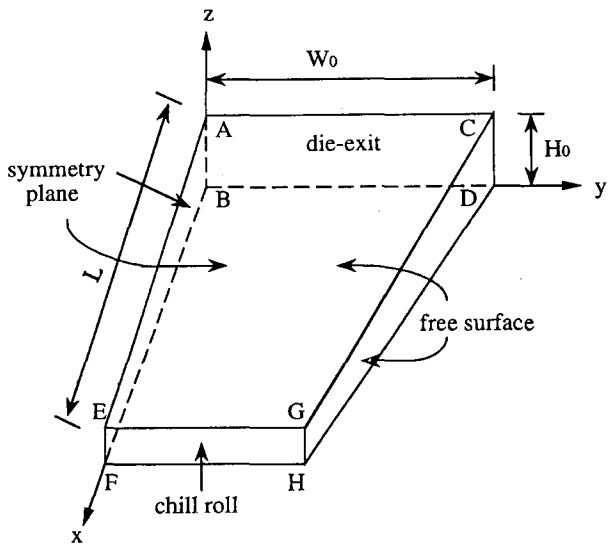

Fig. 2. Flow domain for numerical calculation.

is assumed to be incompressible and only steady flow is considered. The equations governing the flow field are those of continuity and momentum.

$$\nabla \cdot \mathbf{v} = 0 \tag{1}$$

$$\rho \mathbf{v} \cdot \nabla \mathbf{v} = -\nabla p + \nabla \cdot \tau + \mathbf{f} \tag{2}$$

In eqs (1) and (2), $\mathbf{v} = (u,v,w)$ is the velocity vector, p is pressure, τ is the extra stress tensor which is governed by the constitutive equation, $\mathbf{f}$ is the body force per unit volume, and ρ is the density of the fluid.

Polymer solutions in steady shear flow typically exhibit viscosity that decreases with increasing shear rate over a certain range, whereas in steady elongation flow they ordinarily display viscosity that increases with increasing elongational rate. The rheological constitutive equation concerned in this work is a generalized Newtonian model, which is inelastic and concise model being able to represent the shear-thinning and tension-thickening viscosities of polymer solutions. They have the form of

$$\tau = \eta(\dot{\gamma}, \dot{\varepsilon})(\nabla \mathbf{v} + \nabla \mathbf{v}^T) \tag{3}$$

where the viscosity η is a function of shear rate $\dot{\gamma}$ and elongational rate $\dot{\varepsilon}$ of the system. It is well established that the viscosity in steady shear flow can usually be represented by the power-law equation :

$$\eta_{sh} = \eta_o |\dot{\gamma}|^{n-1} \tag{4}$$

Recently it has become evident that the viscosity in steady elongation flow can also be represented by an analogous equation :

$$\eta_{el} = \eta_o |\dot{\varepsilon}|^{m-1} \quad (5)$$

The important features of the model can be investigated by varying the power-law indices n and m.

2.2. Boundary conditions

The boundary is composed of an extrusion line, a free surface and the take-up line at the chill roll. A flow domain is shown schematically in Fig. 2.

The velocity profiles of unidirectional flow and no cross-sectional flow are imposed on the die-exit.

$$u(0,y,z) = u_o, \qquad v(0,y,z) = w(0,y,z) = 0 \quad (6)$$

On the free surface, the velocity component normal to the free surface and the stress component tangential to the free surface vanish.

$$\mathbf{n} \cdot \mathbf{v} = 0 \quad (7)$$

$$\sigma_{nt} = 0 \quad (8)$$

where **n** and **t** are the unit normal and tangent vectors to the free surface. The sheet casting process considered in this work is thought to be affected by surface tension. If the principal radii of curvature of the free surface are R_1 and R_2, the total curvature of the surface is readily established by $1/R_1 + 1/R_2$. If the total curvature of the surface is denoted by 1/R and the normal vector to the surface is oriented outside, then the normal traction σ_{nn} on the curved part of free surface is given by

$$\sigma_{nn} = \frac{\kappa}{R} \quad (9)$$

where κ is the surface tension coefficient.

It is difficult to represent mathematically how real fluids behave at the take-up plane near the chill roll region. Here, we try two types of boundary conditions at the take-up plane. First, it is general to use unidirectional flow condition for the axial velocity and zero cross-sectional flow condition,

$$u(L,y,z) = u_L, \qquad v(L,y,z) = w(L,y,z) = 0 \quad (10)$$

These conditions have been used generally for one- or two-dimensional study in previous literatures on free surface problems. The second set of boundary conditions is

$$u(L,y,z) = u_L, \qquad F_y(L,y,z) = F_z(L,y,z) = 0 \quad (11)$$

It is the representative case of the force-free boundary condition. In this work, we examine the effects of both boundary conditions, eqs (10) and (11) on the numerical simulation. Symmetry conditions are imposed to reduce the size of the problem, where possible (planes ABFE and BDHF in Fig. 2).

3. Numerical method

3.1. Galerkin finite element formulation

Two types of three-dimensional elements are employed for the discretization of the flow domain into finite elements, the 27-node hexahedron and 18-node triangular prism elements. Both elements are isoparametric with triquadratic approximations ψ_i for the velocity components and trilinear approximation ϕ_i for the pressure. And 27 ($3 \times 3 \times 3$) integration points for the hexahedron element and 21 (3×7) integration points for the prism element are used (Lee and Lee, 1990).

After the standard Galerkin procedure is applied, eqs (1) and (2) yield

$$\langle \phi_i ; \nabla \cdot \mathbf{v} \rangle = 0 \quad (12)$$

$$\langle \psi_i ; \rho \mathbf{v} \cdot \nabla \mathbf{v} + \nabla p - \nabla \cdot \tau \rangle = \langle \psi_i ; f_i \rangle \quad (13)$$

where the symbol $\langle \ ; \ \rangle$ stands for the integration over the volume of the system. The resulting Galerkin formulations of eqs (12) and (13) are given in Appendix.

3.2. Free surface update scheme

Free surface flows are nonlinear problems because the position of the free surface is unknown *a priori* and its determination has to be a part of the numerical calculation. The spines are predefined straight lines in space. A base point $\mathbf{x}^i_B$ and a unit vector $\mathbf{e}^i$ determine the spine and the free surface nodes are then given by

$$\mathbf{x}^i_F = \mathbf{x}^i_B + h^i \mathbf{e}^i \quad (14)$$

where the distance h^i is the free surface parameter to be determined, by following the procedure suggested by Kistler and Scriven (1984). The direction $\mathbf{e}^i$ for the displacement of the free surface is defined *a priori* and fixed during the iterative process. However, the direction $\mathbf{e}^i$ is allowed to vary from node to node. The other nodes along the same spine move in the predefined proportions. The spines are allowed to move on y-z plane only at given x coordinate throughout the calculation.

The weighted residual form of the kinematic condition, eq (7), is used to solve the free surface parameters

$$\langle \psi_i ; n_x u + n_y v + n_z w \rangle = 0 \quad (15)$$

and only the elements that have free surface boundary contribute to eq (15). Biquadratic approximation is used for the free surface.

The three-dimensional free surface formulation of sheet casting is faced with the complicating features in

the edge region. To find a location of the highest edge point causes numerical inaccuracy. The highest edge point is hard to be determined accurately unless it lies on a spine. In the spine approach it is found that the global solution is much mesh dependent until the calculation domain has very fine elements, in the vicinity of the edge region.

3.3. Iteration schemes

The Newton-Raphson method is used as an iterative scheme to solve the nonlinear set of governing equations. Equations (12) and (13) with boundary conditions eqs (6)-(11) are solved at each iteration and the resulting systems are solved by the frontal elimination technique. Instead of direct use of the calculated field variables as the next iteration step, a stabilizing relaxation scheme is employed. Relaxation factor ranges between 0.2 and 0.8 depending on the draw ratio of the system. Usually, a lower value of the relaxation factor is employed for a free surface parameter than those for other field variables. A large number of iteration is required, normally 10-80 iterations, inversely proportional to the relaxation factor.

The initial finite element meshes are illustrated in Fig. 3. These meshes are generated by using the commercial finite element program POLYFLOW® and modified in each case based on its continuity. Table 1 gives a detailed measure of the size of problems studied. We keep the total melt drawn length L and the die half-thickness ($H_o = 0.1L$) constant throughout the numerical work. MESH1 is designed to observe uniaxial elongational flow and dimensioned $W_o = 0.2L$, while MESH3 is used to look into mixed (planar and uniaxial) elongational flow, where the die half-width W_o is 7L or 8L. MESH2 is used to observe the intermediate flow behavior between the two extreme cases of MESH1 and MESH3, where the die half-width W_o is 2L or 5L.

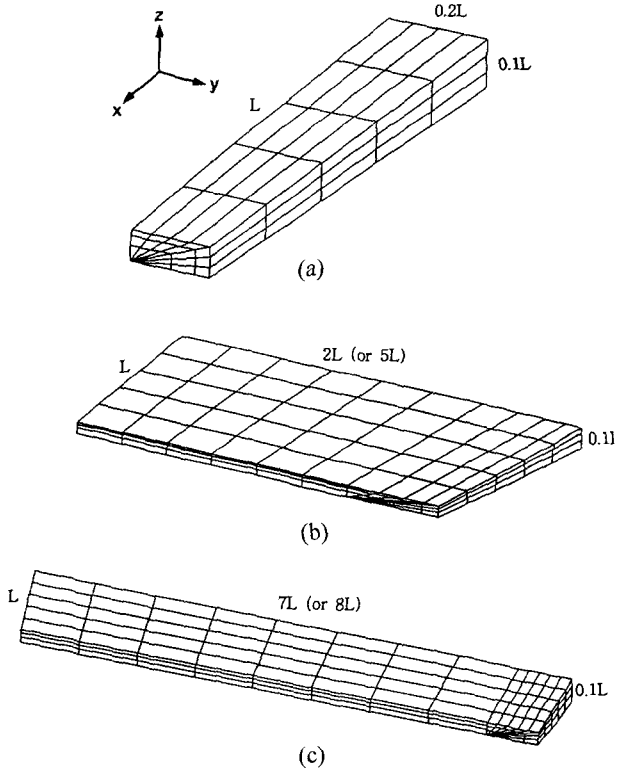

Fig. 3. Perspective view of initial meshes : (a) MESH1, (b) MESH2, (c) MESH3.

Table 1. Size of the problems.

	Elements	Nodes	Variables	Frontal width
MESH1	105	924	3,087	346
MESH2	195	1,848	6,135	356
MESH3	240	2,277	7,554	356

4. Results and discussion

The prime importance of the sheet casting process is to achieve a uniform thickness film at the final products. It has been observed in practice that the sheet forms an edge bead, and periodic variation in thickness profile along the width direction, so called draw resonance. The three-dimensional analysis does not require the additional assumptions usually made in one- or two-dimensional analysis and is expected to give more accurate prediction of the sheet profile.

In this work we consider the degree of neck-in, the bead thickness ratio and the bead width fraction of the final sheet at the chill roll region. The degree of neck-in (NI) represents the percentage of the decrease in the final sheet width to the initial sheet width (see Fig. 2) given as

$$NI = \left(1 - \frac{W_L}{W_o}\right) \times 100 \tag{16}$$

The bead thickness ratio (BT) is defined by the ratio of edge to center thickness of the sheet (see Fig. 4) given as

$$BT = \frac{H_{edge}}{H_{center}} \tag{17}$$

The bead width fraction is arbitrary defined in this study by the percentage of the width between a point of 1.2 times the final center thickness and the end of the edge to the final width (see Fig. 4) given as

$$BW = \frac{W_{edge}}{W_L} \times 100 \tag{18}$$

where the selection of W_{edge} is optional. Using above three parameters, eqs (16)-(18), the following effects of processing conditions are examined.

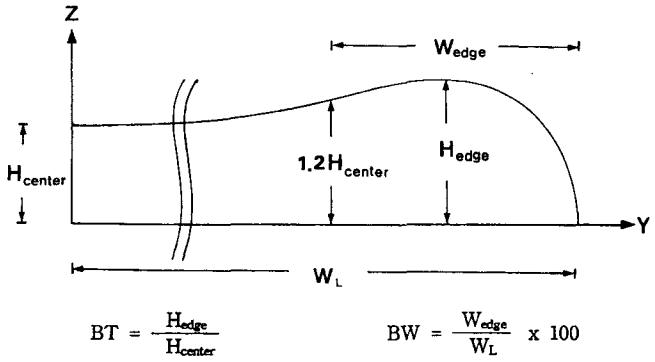

Fig. 4. Sketch of the edge bead section and definitions of bead thickness ratio and bead width fraction.

4.1. Effect of boundary conditions

Sheet casting is a problem which may have stress singularity and this may interrupt the numerical convergence. Accordingly, a proper boundary condition which can alleviate the singular stress is required. If we impose eq (10) on the take-up plane, there appears a sudden change in the boundary condition, from the free surface to zero cross-sectional flow at the take-up plane and this can cause a stress singularity. Fig. 5 shows the pressure distributions obtained along a free surface line at z = 0 (line DH in Fig. 2) at draw ratios of 2 and 4 on MESH1, where solid lines indicate the results of the force-free boundary condition, eq (11), and dashed lines designate the results of zero cross-sectional flow condition, eq (10). It reveals that the pressure difference in the vicinity of chill roll region is large, increases as the draw ratio increases, and is larger in the case of zero cross-sectional flow boundary condition than in the case of force-free boundary condition. The dependence of stress singularity on the boundary condition at the chill roll region is related to the numerical convergence and the domain of convergence can be extended by imposing the force-free boundary condition on the chill roll region. The result implies that this condition is more appropriate in both numerical and physical points of view.

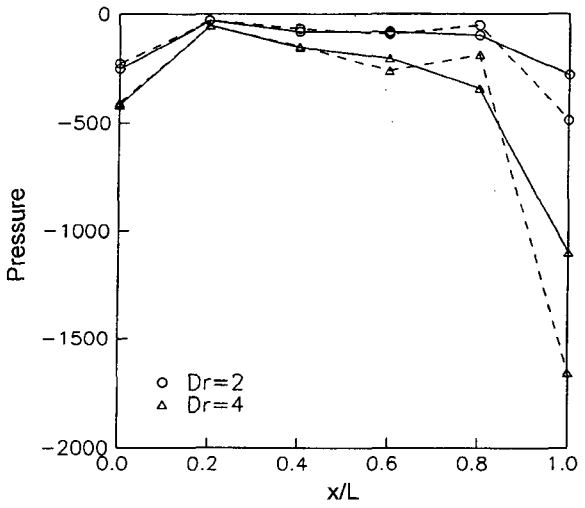

Fig. 5. Effects of two types of boundary conditions at the chill roll on the pressure distribution along DH in Fig. 2 (—: force-free condition, - - - : zero cross-sectional flow condition).

4.2. Effect of draw ratio

The draw ratio (Dr) is one of the most important parameters in sheet casting process. To examine the effect of draw ratio, the fluid inertia, gravity, surface tension, and air drag are ignored. The final sheet profiles at the chill roll region for various draw ratios are shown in Figs. 6-8. In these figures, the ratio of initial width to melt drawn length, W_o/L, is changed from 0.2 to 8 and H_o is fixed to 0.1L. In the case of $W_o/L = 0.2$ shown in Fig. 6, the flow kinematics turns out to be similar to the uniaxial elongational flow, while the flow kinematics shows locally mixed, both uniaxial and planar, elongational flow behaviors when $W_o/L = 8$, as shown in Fig. 8. When the draw ratio increases, the final width decreases and the thickness profile changes such that the edge becomes thick, that is, the bead thick-

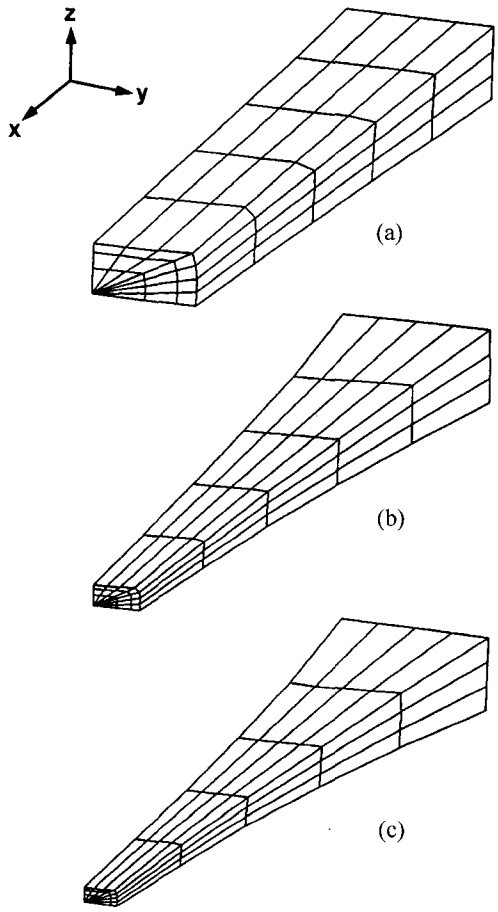

Fig. 6. Perspective view of final meshes for the sheet casting when $W_o/L = 0.2$: (a) Dr = 2, (b) Dr = 10, (c) Dr = 20.

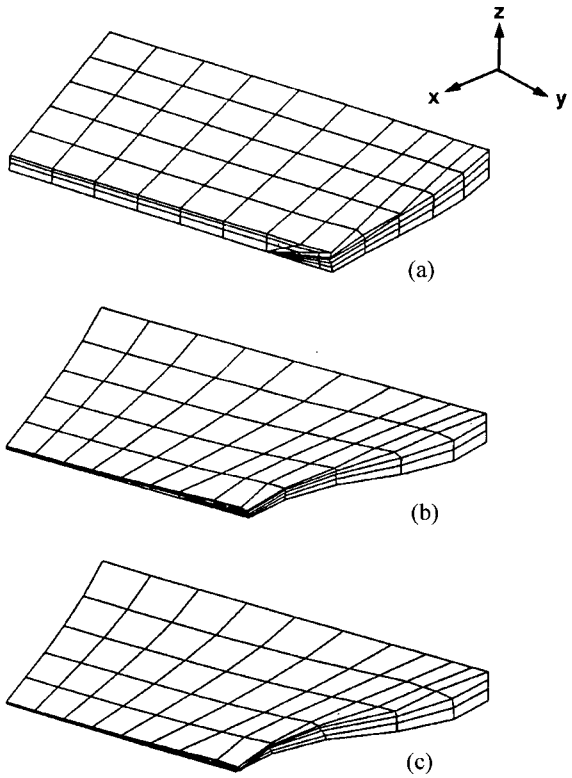

Fig. 7. Perspective view of final meshes for the sheet casting when $W_o/L = 2$: (a) Dr = 2, (b) Dr = 10, (c) Dr = 14.

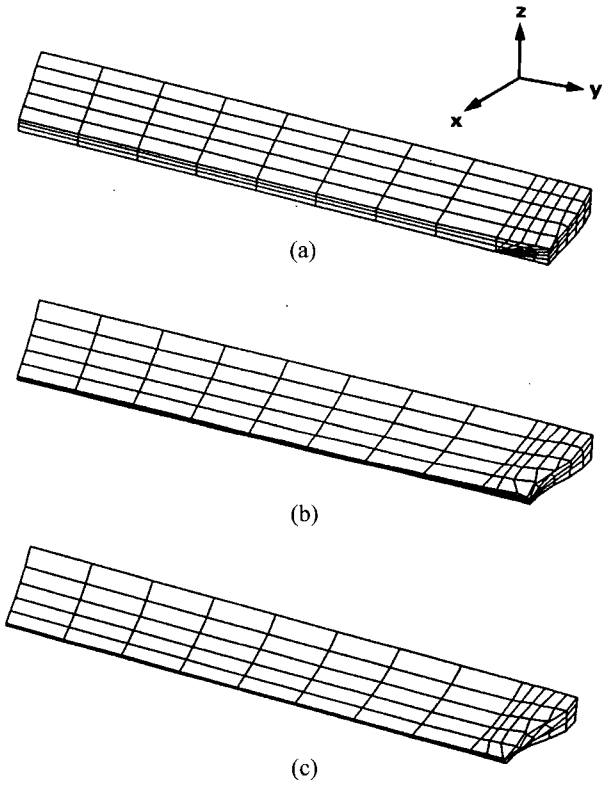

Fig. 8. Perspective view of final meshes for the sheet casting when $W_o/L = 8$: (a) Dr = 2, (b) Dr = 6, (c) Dr = 10.

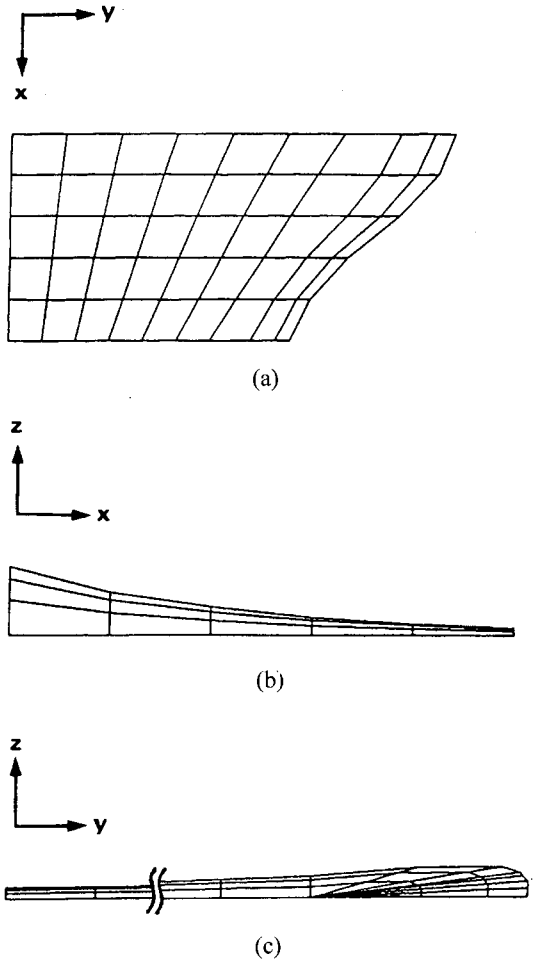

Fig. 9. Two-dimensional view of final sheet profiles when $W_o/L = 2$ and Dr = 10 : (a) sheet width profile at x-y symmetry plane, (b) sheet thickness profile at x-z symmetry plane, (c) sheet thickness profile at the chill roll region.

ness ratio increases. The two-dimensional view of the final sheet profiles in the case of $W_o/L = 2$ and Dr = 10 is shown in Fig. 9. The sheet width at x-y symmetry plane (BDHF plane in Fig. 2) shows S-shaped profile, the sheet thickness at x-z symmetry plane (ABFE plane) shows exponentially decreasing profile, and the sheet thickness at the chill roll region (EFHG plane) shows considerable edge bead profile. The larger the value of W_o/L , the smaller the domain of numerical convergence. Oscillatory behavior of sheet profile is seen along the width at large draw ratios and this is an obstacle to numerical convergence.

In Fig. 10, the degree of neck-in is plotted against the draw ratio for various ratios of W_o/L. The value of draw ratio especially plays a key role on the increase of the degree of neck-in for the low values of W_o/L. Fig. 11 shows the bead thickness ratio as a function of draw ratio for various W_o/L. For the same value of W_o/L, it is found that the bead thickness ratio grows with the draw ratio.

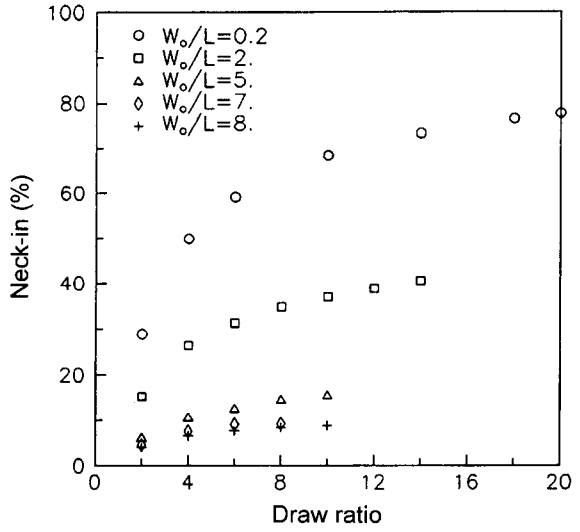

Fig. 10. The degree of neck-in as a function of draw ratio for various W_o/L.

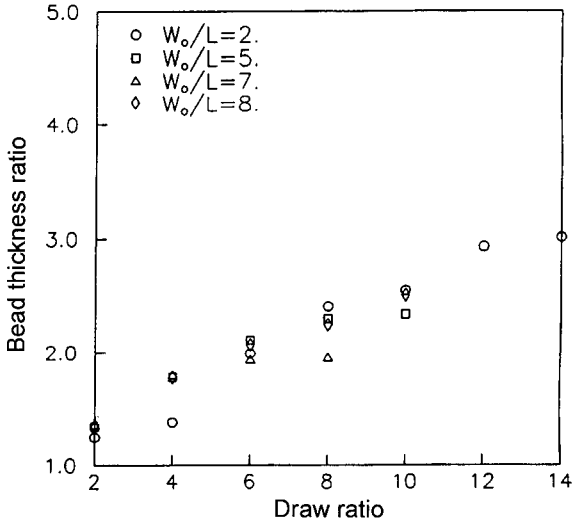

Fig. 11. The bead thickness ratio as a function of draw ratio for various W_o/L.

However, it is difficult to reach quantitative comparisons of bead thickness ratio for various values of W_o/L because these results are obtained from different meshes and the highest edge point does not lie on the spine for some cases. When W_o/L is 0.2 (not shown in Fig. 11), the bead thickness ratio has little effect on the draw ratio and has nearly constant values of 1.03-1.08. The bead width fraction as a function of draw ratio at different values of W_o/L, is shown in Fig. 12. This is dependent on the ratio of W_o/L and decreases as the ratio of W_o/L increases.

In order to examine the effect of initial thickness, the draw ratio and the value of W_o/L are fixed to 6 and 5, respectively. The effects of the degree of neck-in and the bead thickness ratio together with the bead width fraction are examined as a function of the ratio of initial width to

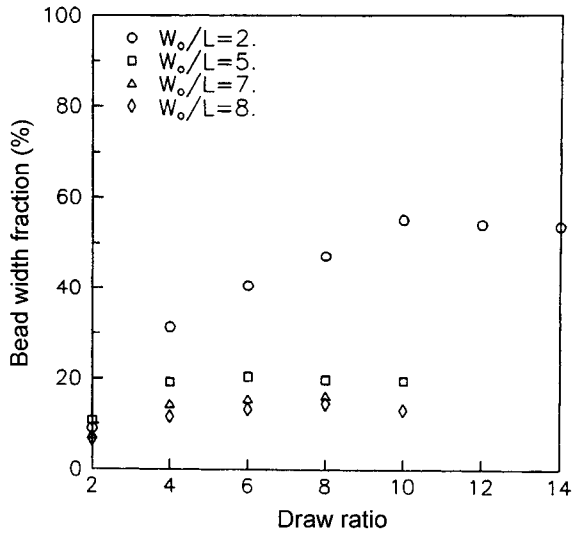

Fig. 12. The bead width fraction as a function of draw ratio for various W_o/L.

initial thickness, W_o/H_o. It is found that the degree of neck-in, the bead thickness ratio, and the bead width fraction are independent of the ratio of W_o/H_o. Therefore, the characteristic dimensionless length parameter determining these effects seems plausible to set to the W_o/L in the range of interest.

4.3. Effects of inertia and gravity

In this section, we would only consider the case of $W_o/L = 2$ and $Dr = 10$. Firstly, in order to consider the effect of inertia, the gravity force and surface tension are assumed to be negligible. Reynolds number in this process which represents the ratio of the inertial to viscous forces is defined as

$$Re = \frac{\rho u_L L}{\eta} \tag{19}$$

Cases up to the Re of 10 have converged. The Reynolds number in sheet casting industry is usually not high and therefore, it seems valid to perform the analysis only up to Re = 10. As shown in Fig. 13, the degree of neck-in and the bead thickness ratio are reduced as Re increases, whereas the bead width fraction has little change. It is found from these results that the inertia exerts a larger effect on the sheet thickness profile than on the sheet width profile.

Secondly, to see the effect of gravity, the sheet is assumed to be extruded in a vertical way from the die-exit as shown in Fig. 1. Thus, the gravity works only in the x-direction. The gravity effect in the viscous flow is usually characterized by the Stokes number, which is the ratio of the gravitational to viscous forces, defined as

$$St = \frac{\rho g L^2}{\eta u_L} \tag{20}$$

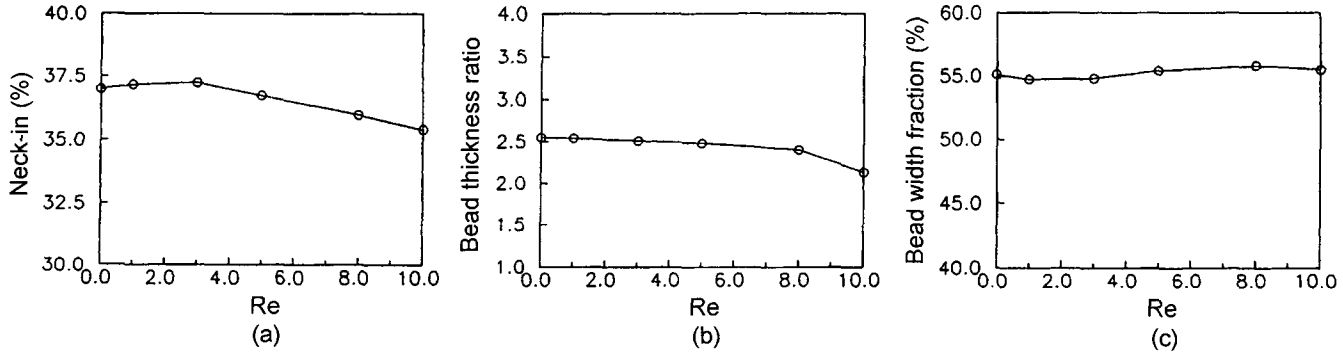

Fig. 13. Dependence of neck-in (a), bead thickness ratio (b), and bead width fraction (c) on the inertia force (characterized as the Reynolds number) when Dr = 10 and $W_o/L = 2$.

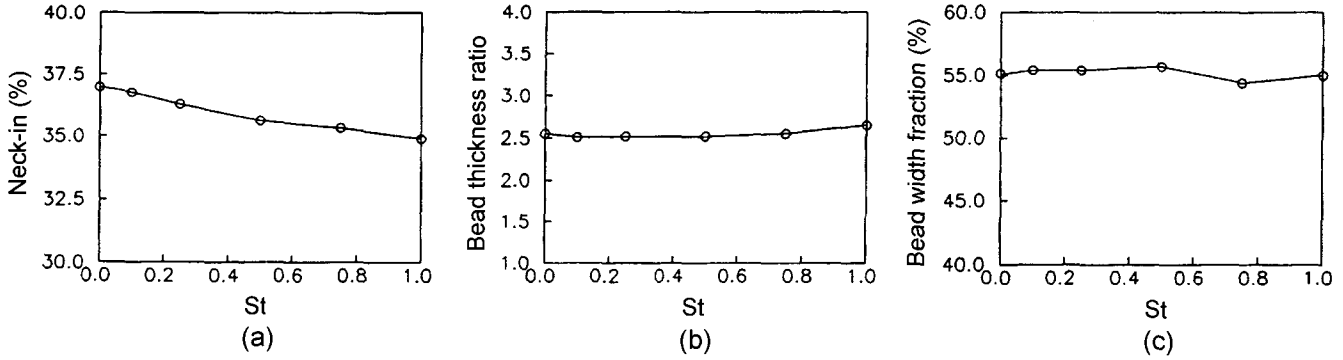

Fig. 14. Dependence of neck-in (a), bead thickness ratio (b), and bead width fraction (c) on the gravity force (characterized as the Stokes number) when Dr = 10 and $W_o/L = 2$.

The numerical computations converged up to St = 1, which corresponds to Re = 0.102. The unstable sheet profile in the width direction is observed even at the low Stokes number. It is uncertain whether this irregularity is attributed to numerical errors or flow instabilities under this condition. Anyway, the numerical results shown in Fig. 14 reveal that the gravity acts to reduce the neck-in and gives little effect on the bead thickness ratio and the bead width fraction.

4.4. Effect of surface tension

Surface tension has been one of the plausible explanations for edge bead formation. The Capillary number which characterizes the ratio of viscous force to surface tension is defined as

$$Ca = \frac{\eta u_L}{\kappa} \tag{21}$$

Keeping all other conditions constant, the Capillary number is changed by varying κ, but the convergence could not be reached for Ca < 1.67. High Capillary number corresponds to low surface tension and presumably, negligible effects on the free surface. At lower capillary numbers, the degree of neck-in and the bead width fraction are smaller and the bead thickness ratio is larger as shown in Fig. 15. This leads to the conclusion that surface tension has little effect on the width profile but large effect on the bead thickness ratio of the sheet. The lower the capillary number, the bigger the edge bead. This agrees with the previous studies in the literature (Dobroth and Erwin, 1986).

4.5. Effect of viscosity function

The behavior of a generalized Newtonian fluid exhibiting the shear-thinning and tension-thickening is examined. The simple power-law model, eq (4), is selected to represent inelastic non-Newtonian behavior of polymer melts. Shear rate is replaced by a function of the second invariant in eq (4) as follows

$$\dot{\gamma} = 2(II_d)^{0.5} \tag{22}$$

Under the assumption of the quasi-elongational approximation (Debbaut and Crochet, 1988; Debbaut *et al.*, 1988; Oh and Lee, 1992), the elongation rate can be expressed by the velocity gradient in eq (5) as follows

$$\dot{\varepsilon} = \frac{du}{dx} \tag{23}$$

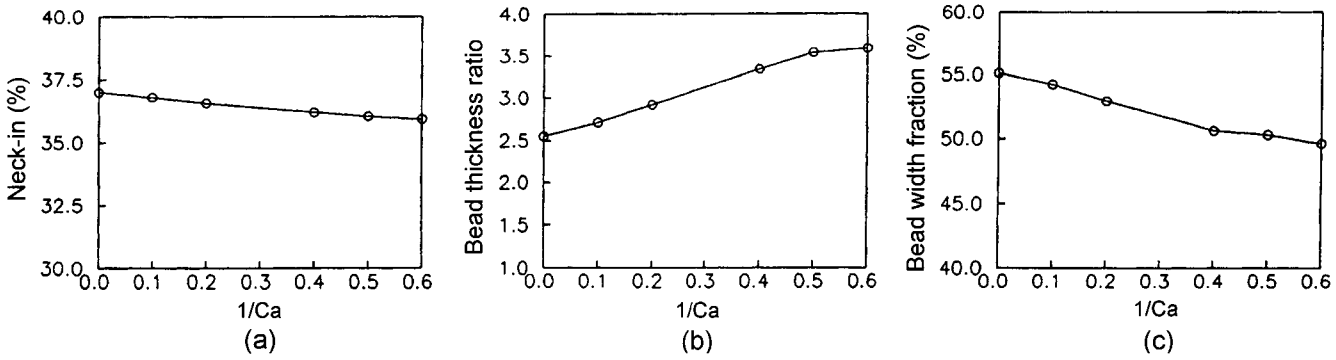

Fig. 15. Dependence of neck-in (a), bead thickness ratio (b), and bead width fraction (c) on the surface tension (characterized as the Capillary number) when Dr = 10 and $W_o/L = 2$.

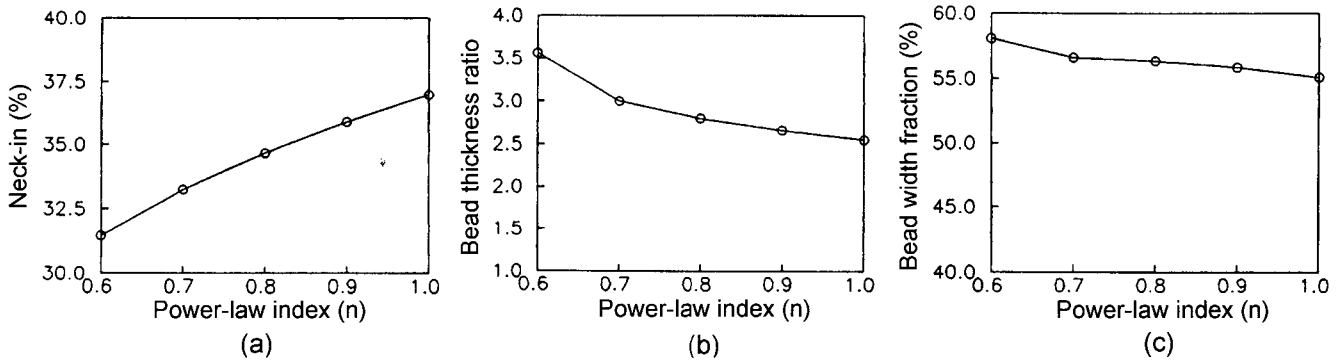

Fig. 16. Dependence of neck-in (a), bead thickness ratio (b), and bead width fraction (c) on the extent of shear-thinning when Dr = 10 and $W_o/L = 2$.

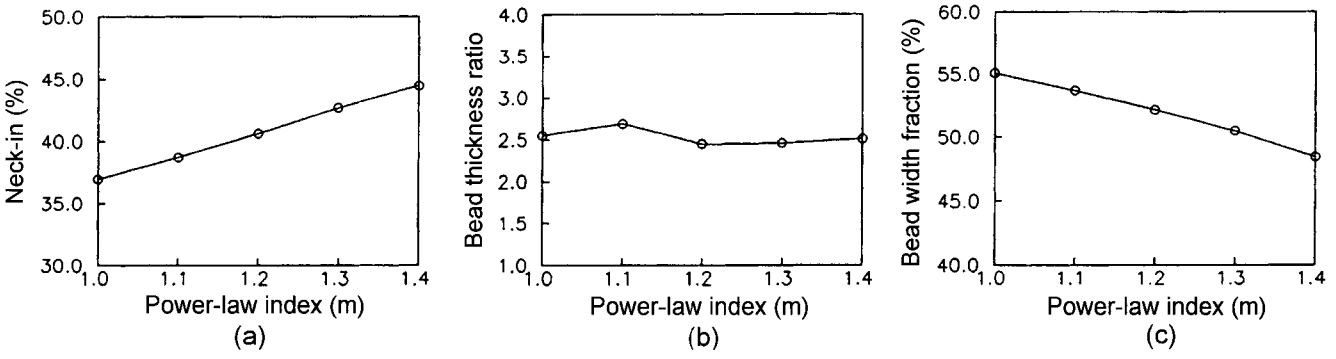

Fig. 17. Dependence of neck-in (a), bead thickness ratio (b), and bead width fraction (c) on the extent of tension-thickening when Dr = 10 and $W_o/L = 2$.

A knowledge for the deformation rate, eqs (22) and (23), provides a measure of the shear-thinning and tension-thickening of the sample. Other factors such as inertia, gravity and surface tension are ignored and the effect of power-law indices is only considered. As can be seen in Fig. 16, numerical results show shear-thinning produces less neck-in and more bead thickness ratio than Newtonian. It has little effect on the bead width fraction. As seen in Fig. 17, the tension-thickening behavior makes the neck-in larger and the bead width fraction smaller. The variation of the bead thickness ratio is negligible.

5. Conclusions

Numerical study on a generalized Newtonian fluid flow in sheet casting process has been performed by the three-dimensional finite element method. Imposing a force-free boundary condition on the chill roll region greatly facilitates to obtain a converged solution and get close to the practical state of processing. Inertia, gravity and surface tension slightly reduce the degree of neck-in. In view of bead thickness ratio, surface tension tends to make larger but inertia exerts a small negative effect. The most influ-

ential factor for large bead thickness ratio is surface tension. In the flow behavior of a generalized Newtonian fluid, the tension-thickening effect produces larger neck-in and smaller bead width fraction than those in the Newtonian fluid.

Nomenclature

$\mathbf{e}^i$: unit vector
$\mathbf{f}$: body force per unit volume
g : gravitational acceleration constant
h^i : free surface parameter
H_o : initial half thickness of the die
II_d : second invariant of the rate of deformation tensor
L : melt drawn length
m,n : power-law index
$\mathbf{n}$: outward unit normal vector
p : pressure
R : total radius of curvature
$\mathbf{t}$: outward unit tangential vector
u_L : take-up velocity
u_o : die-exit velocity
$\mathbf{v}$: velocity vector
u,v,w : velocity components in x, y, z directions
W_L : final half width of the sheet
W_o : initial half width of the die
x,y,z : global coordinates

Greek letters

$\dot{\gamma}$: shear rate
$\dot{\varepsilon}$: elongation rate
η : viscosity
η_o : zero-shear viscosity
κ : surface tension
ρ : density
σ_{nn} : normal stress to the free surface
σ_{nt} : tangential stress to the free surface
τ : extra stress tensor
ϕ_i : bilinear or trilinear interpolation function
ψ_i : biquadratic or triquadratic interpolation function

Appendix

The final forms of Galerkin equations are given by

$$\langle \psi_{i,x} ; -p+2\eta u_{,x} \rangle + \langle \psi_{i,y} ; \eta(u_{,y} + v_{,x}) \rangle + \langle \psi_{i,z} ; \eta(u_{,z} + w_{,x}) \rangle + \rho \langle \psi_i ; uu_{,x} + vu_{,y} + wu_{,z} \rangle = \langle \psi_i ; f_x \rangle + \langle\langle \psi_i ; t_x \rangle\rangle \quad (A.1)$$

$$\langle \psi_{i,x} ; \eta(u_{,y} + v_{,x}) \rangle + \langle \psi_{i,y} ; -p+2\eta v_{,y} \rangle + \langle \psi_{i,z} ; \eta(v_{,z} + w_{,y}) \rangle + \rho \langle \psi_i ; uv_{,x} + vv_{,y} + wv_{,z} \rangle = \langle \psi_i ; f_y \rangle + \langle\langle \psi_i ; t_y \rangle\rangle \quad (A.2)$$

$$\langle \psi_{i,x} ; (\eta u_{,z} + w_{,x}) \rangle + \langle \psi_{i,y} ; \eta(v_{,z} + w_{,y}) \rangle + \langle \psi_{i,z} ; -p+2\eta w_{,z} \rangle + \rho \langle \psi_i ; uw_{,x} + vw_{,y} + ww_{,z} \rangle = \langle \psi_i ; f_z \rangle + \langle\langle \psi_i ; t_z \rangle\rangle \quad (A.3)$$

$$\langle \phi_i ; u_{,x} + v_{,y} + w_{,z} \rangle = 0 \quad (A.4)$$

where the symbol $\langle\langle\ ;\ \rangle\rangle$ stands for the integration over the boundary surface, and t_x, t_y and t_z are the x, y and z components of the contact force vector, respectively. Substituting the corresponding shape functions to eqs (A.1)-(A.4) and reorganizing the system of equations in terms of u, v, w and p, the following forms of the nonlinear algebraic system of equations are constructed.

$$A_{ij}u_j + D_{ij}v_j + E_{ij}w_j + IX_{ijk}u_ju_k + IY_{ijk}v_ju_k + IZ_{ijk}w_ju_k - PX_{ij}p_j = X_i \quad (A.5)$$

$$D_{ji}u_j + B_{ij}v_j + F_{ij}w_j + IX_{ijk}u_jv_k + IY_{ijk}v_jv_k + IZ_{ijk}w_jv_k - PY_{ij}p_j = Y_i \quad (A.6)$$

$$E_{ji}u_j + F_{ji}v_j + C_{ij}w_j + IX_{ijk}u_jw_k + IY_{ijk}v_jw_k + IZ_{ijk}w_jw_k - PZ_{ij}p_j = Z_i \quad (A.7)$$

$$-PX_{ji}u_j - PY_{ji}v_j - PZ_{ji}w_j = 0 \quad (A.8)$$

where

$$A_{ij} = 2\langle \eta\psi_{i,x} ; \psi_{j,x} \rangle + \langle \eta\psi_{i,y} ; \psi_{j,y} \rangle + \langle \eta\psi_{i,z} ; \psi_{j,z} \rangle$$

$$B_{ij} = \langle \eta\psi_{i,x} ; \psi_{j,x} \rangle + 2\langle \eta\psi_{i,y} ; \psi_{j,y} \rangle + \langle \eta\psi_{i,z} ; \psi_{j,z} \rangle$$

$$C_{ij} = \langle \eta\ \psi_{i,x} ; \psi_{j,x} \rangle + \langle \eta\ \psi_{i,y} ; \psi_{j,y} \rangle + 2\langle \eta\psi_{i,z} ; \psi_{j,z} \rangle$$

$$D_{ij} = \langle \eta\ \psi_{i,y} ; \psi_{j,x} \rangle \qquad E_{ij} = \langle \eta\ \psi_{i,z} ; \psi_{j,x} \rangle$$

$$F_{ij} = \langle \eta\ \psi_{i,z} ; \psi_{j,y} \rangle \qquad PX_{ij} = \langle \psi_{i,x} ; \phi_j \rangle$$

$$PY_{ij} = \langle \psi_{i,y} ; \phi_j \rangle \qquad PZ_{ij} = \langle \psi_{i,z} ; \phi_j \rangle$$

$$IX_{ijk} = \langle \rho\psi_i ; \psi_j\psi_{k,x} \rangle \qquad IY_{ijk} = \langle \rho\psi_i ; \psi_j\psi_{k,y} \rangle$$

$$IZ_{ijk} = \langle \rho\psi_i ; \psi_j\psi_{k,z} \rangle$$

The finite element solution of a generalized Newtonian flow is obtained by solving the nonlinear algebraic system consisting of eqs (A.5)-(A.8).

Acknowledgement

Seong Jong Lee would like to thank the Korean Ministry of Education for the financial aid through the Brain Korea 21 Project.

References

Alaie, S.M. and T.C. Papanastasiou, 1991, Film casting of vis-

coelastic liquid, *Polym. Eng. Sci.* **31**, 67.
Anturkar, N.R. and A. Co, 1988, Draw resonance in film casting of viscoelastic fluids: A linear stability analysis, *J. Non-Newtonian Fluid Mech.* **28**, 287.
Debbaut, B. and M.J. Crochet, 1988, Extensional effects in complex flows, *J. Non-Newtonian Fluid Mech.* **30**, 169.
Debbaut, B. and J.M. Marchal, 1995, Viscoelastic effects in film casting, *Z. Angew Math. Phys.* **46**, 679.
Debbaut, B., M.J. Crochet, H. Barnes and K. Walters, 1988, Extensional Flows of Inelastic Liquids, Proc. Xth Int. Congress Rheology, Sydney, **1**, 291.
d'Halewyn, S., J.F. Agassant and Y. Demay, 1990, Numerical simulation of the cast film process, *Polym. Eng. Sci.* **30**, 335.
Dobroth, T. and L. Erwin, 1986, Causes of edge beads in cast films, *Polym. Eng. Sci*, **26**, 462.
Kistler, S.F. and L.E. Scriven, 1984, Coating flow theory by finite element and asymptotic analysis of the Navier-Stokes system, *Int. J. Num. Meth. Fluid*, **4**, 207.
Lee, S.J. and S.J. Lee, 1990, Numerical prediction of three-dimensional extrudate swell, *Korean J. Rheol.* **2**, 35.
Oh, J.H. and S.J. Lee, 1992, A rheological study on the viscoelastic flow past spheres in a cylinder, *J. Materials Processing and Manufacturing Sci*, **1**, 3.
Silagy, D., Y. Demay and J.F. Agassant, 1999, Numerical simulation of the film casting process, *Int. J. Num. Meth. Fluid*, **30**, 1.
Song, K.S., 1993, Two Dimensional Numerical Study on Film Casting Process, MS thesis, Seoul National University, Korea.
Yeow, Y.L., 1974, On the stability of extending films: A model for the film casting process, *J. Fluid Mech*, **66**, 613.